

Lab on a Chip

Accepted Manuscript



This is an *Accepted Manuscript*, which has been through the Royal Society of Chemistry peer review process and has been accepted for publication.

Accepted Manuscripts are published online shortly after acceptance, before technical editing, formatting and proof reading. Using this free service, authors can make their results available to the community, in citable form, before we publish the edited article. We will replace this *Accepted Manuscript* with the edited and formatted *Advance Article* as soon as it is available.

You can find more information about *Accepted Manuscripts* in the [Information for Authors](#).

Please note that technical editing may introduce minor changes to the text and/or graphics, which may alter content. The journal's standard [Terms & Conditions](#) and the [Ethical guidelines](#) still apply. In no event shall the Royal Society of Chemistry be held responsible for any errors or omissions in this *Accepted Manuscript* or any consequences arising from the use of any information it contains.

On-Chip Sample Preparation for Complete Blood Count from Raw BloodJohn Nguyen¹, Yuan Wei¹, Yi Zheng^{1,2}, Chen Wang^{4,5*}, and Yu Sun^{1,2,3*}¹Department of Mechanical and Industrial Engineering, University of Toronto, Toronto, ON, Canada²Institute of Biomaterials and Biomedical Engineering, University of Toronto, Toronto, ON, Canada³Department of Electrical and Computer Engineering, University of Toronto, Toronto, ON, Canada⁴Department of Pathology and Laboratory Medicine, Mount Sinai Hospital, Toronto, ON, Canada⁵Department of Laboratory Medicine and Pathobiology, University of Toronto, Toronto, ON, Canada

*Corresponding authors:

Yu Sun

E-mail: sun@mie.utoronto.ca

Tel: 1-416-946-0549

Fax: 1-416-978-7753

Chen Wang

E-mail: cwang@mtsinai.on.ca

Tel: 1-416-586-4469

Abstract

This paper describes a monolithic microfluidic device capable of on-chip sample preparation for both RBC and WBC measurements from whole blood. For the first time, on-chip sample processing (e.g. dilution, lysis, and filtration) and downstream single cell measurement were fully integrated to enable sample preparation and single cell analysis from whole blood on a single device. The device consists of two parallel sub-systems that perform sample processing and electrical measurements for measuring RBC and WBC parameters. The system provides a modular environment capable of handling solutions of various viscosities by adjusting the length of channels and precisely controlling mixing ratios, and features a new ‘offset’ filter configuration for increased duration of device operation. RBC concentration, mean corpuscular volume (MCV), cell distribution width, WBC concentration and differential are determined by electrical impedance measurement. Experimental characterization of over 100,000 cells from 10 patient blood samples validated the system’s capability for performing on-chip raw blood processing and measurement.

Keywords

On-chip sample preparation, whole blood, monolithic, complete blood count (CBC), red blood cells, enumeration, white blood cell differential.

Introduction

Blood constituents consist of proteins, glucose, mineral ions, hormones and blood cells including red blood cells (RBCs or erythrocytes), white blood cells (WBCs or leukocytes) and platelets¹. The enumeration and characterization of these blood cell constituents can provide important clinical insight. For example, an abnormally low RBC concentration² is a characteristic of insufficient oxygen delivery and can be indicative of potential disorders such as anemia^{3,4} and leukemia.^{4,5} WBCs play a vital role in immune response to infection and foreign bodies. Measuring WBCs can be a preliminary step in the diagnosis of a number of conditions such as inflammatory processes, bone marrow alterations, and immune disorders^{1,4}. Platelets and their concentration can be used to assess the body's clotting ability.¹

In whole blood, RBCs outnumber WBCs by a ratio of 1000:1,² making it challenging to distinguish between target cell groups and remaining blood cell population. Hence, sample preparation to either sort, concentrate, isolate or separate target blood cells is necessary to facilitate downstream measurement. Conventional approaches of blood cell separation are limited by the required blood sample volume, cell quality, processing time, operation efficiency and variability. The objective of sample preparation for analysis of WBCs and RBCs differ vastly. RBCs constitute roughly 45% of raw blood by volume, making distinguishing single RBCs from the residual population difficult without dilution. Dilution for RBC analysis while straightforward can be technically difficult due to the required scale of dilution. This necessitates large sample volumes, and/or serial dilution steps which contribute to an accumulation of non-systematic errors making approximation of the native RBC concentration nontrivial.

Similarly, the isolation of WBCs and the depletion of contaminating RBCs are critical for analysis to eliminate RBCs' masking effect. In laboratory settings, these cell sorting methods include the use of antibodies and their specificity to surface protein markers on target blood cells such as WBCs.⁶ These techniques have advantages of high specificity and sensitivity but are limited by their operational complexity induced by multi-step sample preparation and incubation time required for antibody binding.

More readily available methods for WBC isolation are differential centrifugation and selective bulk lysis targeting RBCs. However, centrifugation typically results in low separation resolution and has poor versatility in its target cell groups. For bulk lysis, bench-top procedures suffer from non-uniform lysis conditions, mixing and diffusion times and thus, can affect cell populations and introduce variability in downstream analysis results. Overall, these conventional methods for raw blood dilution and isolation are macroscale in nature and are constrained by large sample volumes and several manual processing steps. They also commonly require skilled users and costly/bulky equipment.

Microfluidics can address these issues to reduce time and costs of sample preparation while enabling integrated measurements for real-time monitoring and providing immediate access to critical information for point-of-care applications. Microfluidic separation mechanisms leveraging inherent differences in cell size and density have been used ranging from physical filtration⁷⁻¹⁰, to hydrodynamic¹¹⁻¹⁵ and hemodynamic mechanisms¹⁶⁻¹⁸. These technologies typically have specific flow rate requirements to perform optimally. Thus, the integration with downstream analysis amplifies overall complexity by inheriting flow rate requirements of all involved modules.

Lysis using established protocols¹⁹ can be implemented on microfluidic devices, allowing for repeatable and uniform control over fluidic conditions and minimizing alteration to cellular phenotype. A single stage lysis protocol for continuous in-flow lysis of RBCs has been demonstrated²⁰⁻²². More complex multi-stage protocols using lysis and quench steps have been shown to be effective in lysing RBCs and increasing the discrimination of WBC subtypes.²³⁻²⁶ Complete blood count, the most commonly conducted medical test, requires the enumeration and analysis of blood constituents including both RBCs and WBCs. However, many of the aforementioned technologies neglect RBCs in their analysis and are lacking in a platform for both RBC and WBC sample preparation. Van Berkel et al. demonstrated a platform for complete sample preparation, but the platform lacks on-chip integration of analysis necessitating multiple specialized devices and manual intervention for sample transfer²⁶.

Here, we report a fully monolithic microfluidic device capable of performing blood sample preparation for downstream on-chip RBC and WBC analysis. As a demonstration of our processing capabilities, the device integrates on-chip sample preparation and single cell electrical impedance measurement on a compact platform producing complete blood count information from whole blood. Robust fluidic handling of whole blood is enabled by integrated dilution, lysis, quench, filtration and electrical analysis. Our channel network design based on analogous circuit modeling simplifies microfluidic device design and enables all fluidic flow to be driven by a single pneumatic pressure source. The use of a single pneumatic pressure source reduces bulk and operational complexity. Integrated filtration permits the measurement of over 10,000 cells in each analysis module for obtaining statistically significant sample sizes. The experimental duration is approximately 20-25 minutes, depending on the initial concentration of the sample. The device's complete functionality (i.e., dilution, lysis, filtration, and measurement), compactness and simplicity of measurement enable reliable enumeration and characterization of both RBCs and WBCs immediately downstream of sample preparation.

System Overview

The device uses integrated coulter counters for downstream electrical enumeration and analysis in continuous flow after sample preparation. The device operates in a parallel fashion, siphoning raw/whole blood from a single sample inlet into two separate streams for concurrent RBC and WBC processing and measurement [Fig. 1(A)]. Parallel sample processing is necessary to achieve required dilution ratios as dictated by measurement requirements (1:10,000 for RBCs) and lysis protocols (1:23 for WBCs).

In Coulter counter measurement, 'coincident events' also known as 'coincidence' is the consequence of multiple objects simultaneously present in the detection region, making accurate enumeration difficult. Dilution can reduce the number of coincident events from the overwhelmingly large concentration of RBCs (3,500-5,000 cells/ μL) in raw blood. To achieve optimal dilution for RBC

analysis, four separate 1:10 dilution modules are serially employed before the sample reaches in-line filtration modules [Fig. 1(E)]. In each module, sample flow is merged with diluent in a 1:10 ratio before flowing through a long serpentine mixing channel. A portion of flow is then siphoned off to waste to prepare for the next dilution module. For large scale microfluidic dilution, two prevalent configurations are pyramidal and serial.²⁷⁻³⁰ Here, serial dilution is used preferred to limit overall fluidic flow required and system bulk. A modified serial dilution scheme employing multiple inlets of similar solutions is used in our device design [right side of Fig. 1]. Each dilution module connects to its own individual buffer and waste outlet allowing flexible modifications to overall operation. Two examples of modifications are, firstly, to introduce different buffer solutions at various inlets for multiple solution mixing and secondly, to reduce the intended dilution ratio by dead-ending both inlets and outlets.

To properly analyze WBCs, sample lysis and quench [Fig. 1(B)] is necessary for removing RBCs due to the large density discrepancy between RBCs and WBCs [see ESI video S1]. Saponin/formic acid lysis is preferred over similar chemical protocols using ammonium chloride or osmotic lysis due to its rapid acting nature and its ability to increase WBC subtype discrimination. Saponin has been shown to slightly alter intracellular electrical properties (e.g., membrane permittivity); however, inherent size differences between specific WBC subgroups are distinguishable³¹. This potentially unlocks 3-WBC differential capabilities comparable to other systems using proprietary solutions. Following lysis, flow is filtered and before finally undergoing electrical measurement (10-990 kHz) in the constriction region [Fig. 1(D)]. In cases where lysis is not 100% complete, the minute remaining RBC population can be easily distinguished from WBCs. The size difference between WBCs and RBCs is substantial to differentiate the two cell types (10-15 μm for WBCs vs. 6.2-8.2 μm for RBCs)^{32,33}. This difference is even more pronounced under flow conditions due to RBCs' folding deformation resulting in even lower electrical volume^{34,35}. Fig. 2 shows representative experimental data highlighting the effective electrical volume difference between the two cell groups. Platelet concentration is unobserved here as their size lies below the limit of detection for current device geometries. To properly design constriction channels for electrical

measurement, the dimensions of constriction channels should be sufficiently large to avoid physical squeezing cells to ensure precise size correlation from electrical measurement, and not overly large as to affect electrical detection limits and size resolution for target cell groups. [see ESI Fig. 1].

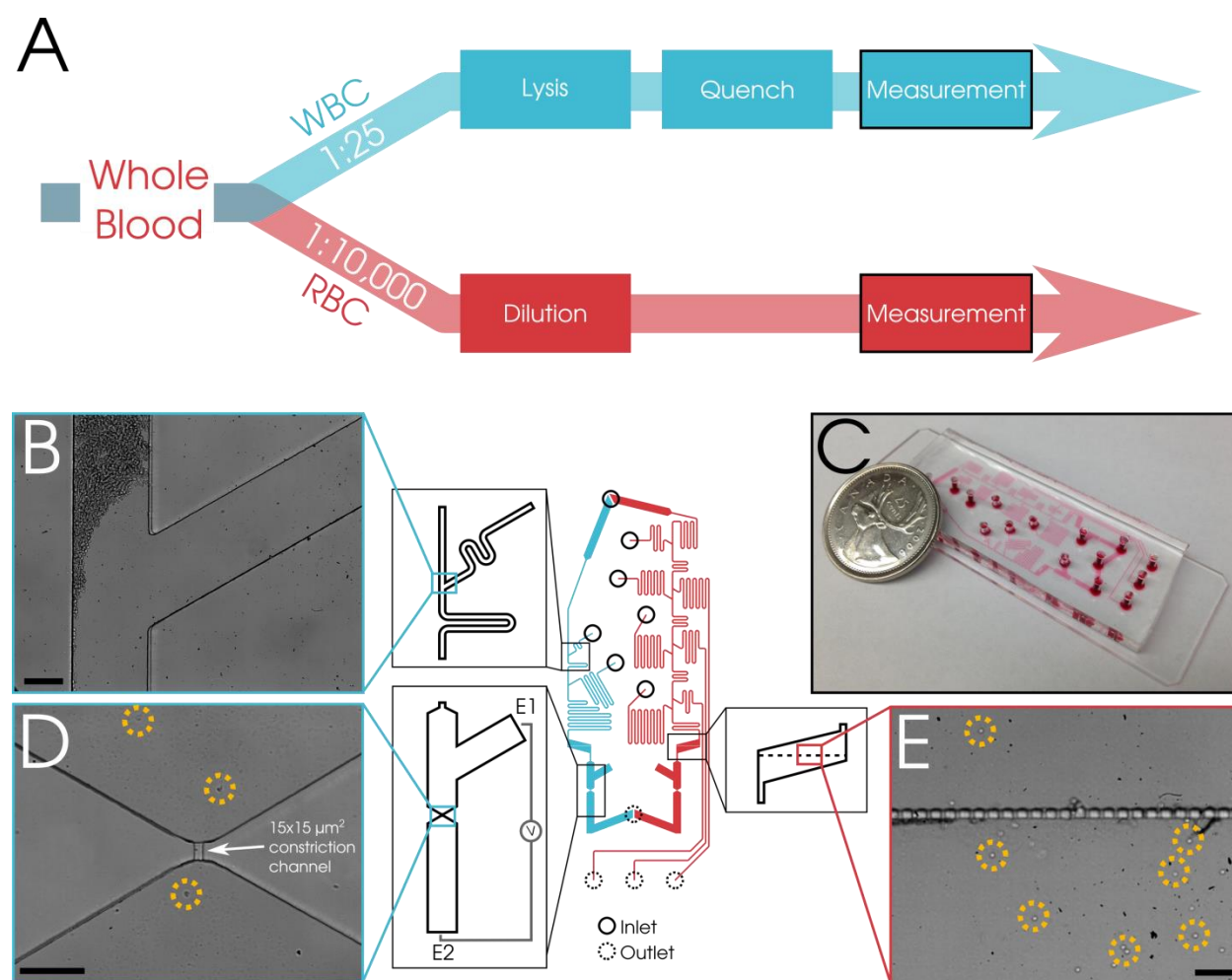


Fig. 1 Schematic highlighting key modules for RBC (red) and WBC (blue) processing. (A) Flow schematic highlighting flow through device for RBC and WBC sample preparation protocols. Also highlighted are necessary dilution ratios, 1:25, 1:10,000 for WBC and RBC measurement, respectively. (B) Module used to lyse RBCs with lysis solution. (C) Fully monolithic microfluidic device for blood cell sample preparation on $18 \times 48 \text{ mm}^2$ footprint. (D) Downstream electrical measurement with electrode

positions denoted E1 and E2. WBCs are circled. (E) Inline filtration modules used to eliminate debris positioned directly before each constriction channel and downstream of dilution and lysing modules for RBC and WBC measurement. RBCs are circled. Filtration and measurement modules are identical for both RBC and WBC analysis. All scale bars represent 100 μm .

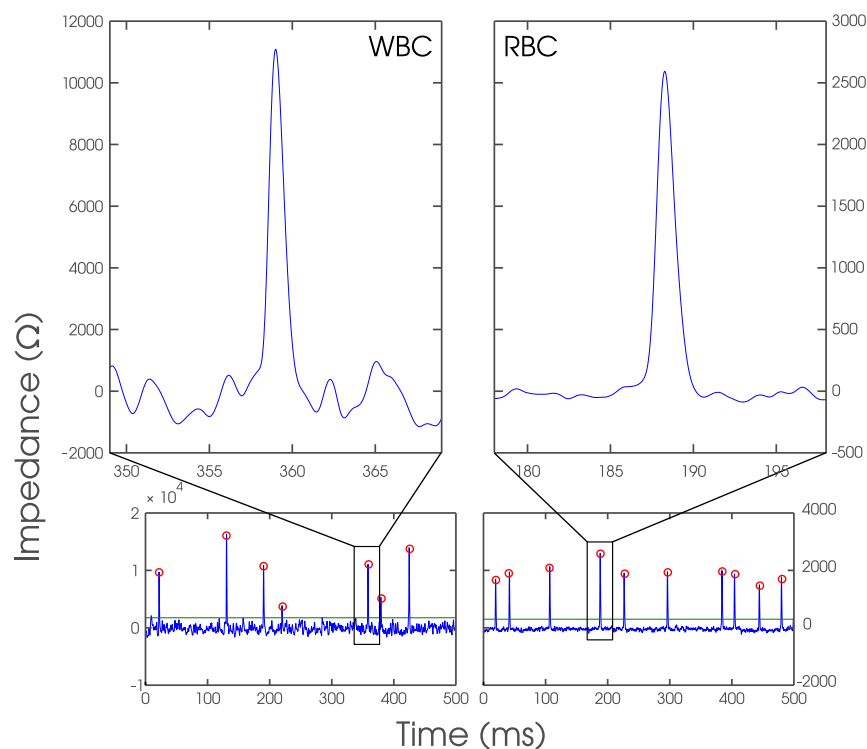


Fig. 2 Two 500 ms segments of raw data showing detection threshold (green line) and enumerated cells (circled red). Data also highlight effective electrical volume difference between WBCs (left) and RBCs (right).

Device Design

The relative ratio of flow rates of buffer, sample, lysis and quench is fixed by the desired dilution ratio and established lysis protocols¹⁹. The large number of fluidic processes and the complexity of the network require the use of an electrical circuit analogy particularly for reducing fluidic flow sources. We

derived analytical solutions describing fluid flow from equivalent circuit equations, which conveniently reduce to a system of linear algebraic equations³⁶.

As illustrated in Fig. 3(A) an analogous circuit model is used in our work to generate specific mixing ratios, incubation time and preferred flow rates. The fluidic resistance of a rectangular microfluidic channel is $R_h \cong \frac{12\mu L}{wh^3(1-0.63\frac{h}{w})}$ provided that the channel width is much larger than its height (i.e., $w \gg h$).³⁷ If the cross sectional dimensions of all channels and fluid viscosity μ are constant, the approximation can be reduced to the product of a summarized coefficient α and the channel length, $R_h \cong \alpha L$. Channel lengths can be used instead of the more physically applicable but more unwieldy fluidic resistances [$\text{Pa}\cdot\text{s}/\text{m}^3$] as resistor values in the circuit model. Here, all fluidic handling channels are $200 \mu\text{m} \times 40 \mu\text{m}$ as a compromise between minimizing fluidic resistance and maximizing device compactness. In cases where the channel function (e.g., constriction channels and filtration modules) demanded variation in the cross sectional dimension or fluidic viscosities (e.g., buffer and whole blood), a comparable channel length of standardized dimensions and equivalent fluidic resistance was used as a model input. In our device for blood processing, viscosities of raw blood and solutions can vary greatly. Blood viscosity is approximately 5.3 times greater than that of buffer solution³⁸ (5.3 Pa·s vs. 1 Pa·s). Consequently, resistor values in the circuit model can be scaled by this difference in viscosity to reflect differences in α between channels handling whole blood and buffer solution. Closed form equations obtained from circuit analysis of Fig. 3(A) are iteratively solved to yield channel lengths for various fluidic resistors (e.g., R_i ; lysis resistor, $R_{b,I}$; dilution buffer 1 and $R_{w,I}$; dilution waste 1) to ensure specific mixing/dilution ratios [see ESI Fig. 2].

RBC and WBC processing modules are operated simultaneously with a single pressure source. This has advantages in terms of portability and compactness over microfluidic devices requiring stringent and bulky flow rate control, and typically requiring an individual source for each solution (e.g., lysis solution, dilution buffer, and quench solution). In addition, the short total channel length and hence lower pressure

requirement of our device compared to other devices^{27,28} makes the device more suited for portable applications especially since the operation pressure of 1.5 kPa is easily attainable without the need of compressed gases and additional cumbersome equipment.

Our technique of using an electric circuit analogy permits the design of microfluidic networks that are independent of flow rates, applied pressure, mixing ratios (d_r) and viscosities. The modified serial dilution scheme designed via circuit analogies allows for a modular system capable of adjusting multiple mixing solutions and ratios after device construction. By scaling channels of various dimensions, functions and viscosities to a length of standardized dimensions, we address limitations of existing pressure driven microfluidic devices. Users can capitalize on the versatility of both the device design process and operation to develop complex microfluidic systems capable of handling a high number of tasks.

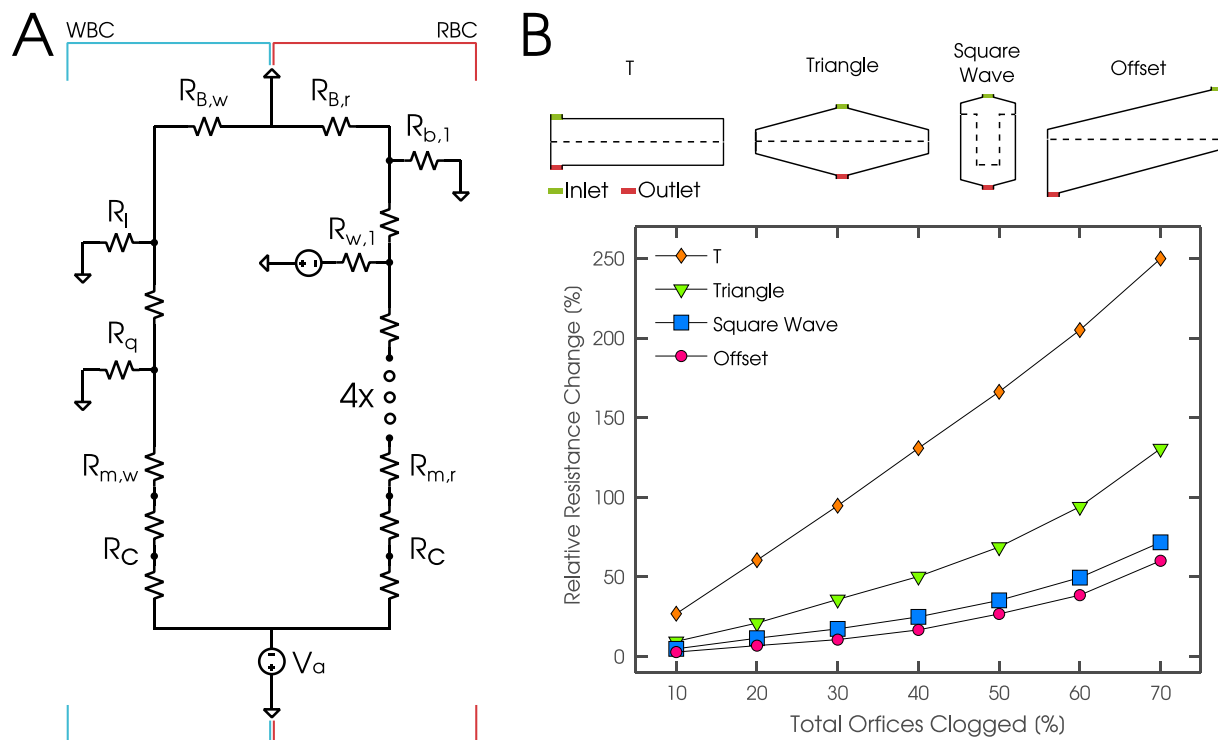


Fig. 3 Design methodology. (A) Fluidic analogous circuit model used to determine channel geometries and configuration to ensure precise fluidic mixing ratios. Subscripts denote fluidic resistors in various

modules (B: blood, b: buffer, w: waste, l: lysis, q: quench, m: mixing and C: constriction). (B) Figure summarizes simulation results comparing unwanted fluidic resistance change as increasing percentage of orifices becoming clogged for existing and our new offset filter configurations. When 50% of filter orifices become clogged, our offset filter increases fluidic resistance only by 26.8%.

Filter design and implementation

Single Coulter counter measurement of cells requires channel dimensions to be comparable to cell size in order to obtain a high cell to detection volume ratio. Debris can plague the use of constriction channels, and debris can vary in size, deformability and material make-up. The lysis of RBCs is rarely 100% debris free and produces highly deformable RBC ghosts which are remnant RBC membranes without internal components.³⁹ Individually RBC ghosts can freely travel but can cluster and collectively impede electrical measurements by clogging the constriction channel. Increasingly higher negative pressure can be applied to dislodge the clog but due to the porous nature of a debris cluster, removing the clog by applying high pressure is not always effective. Thus filtration is a necessary module in sample preparation for single cell analysis. By forcing the sample flow through the array of orifices of comparable sizes³⁹⁻⁴¹, the usage of an in-line filtration module positioned downstream of the fluidic mixing modules, can significantly reduce the occurrences of constriction channel clogging, which is crucial for extending experiment duration. The filter modules summarized in Fig. 3(B) possess similar working principles of forcing samples to flow through arrays of small orifices of comparable size to the downstream constriction channel.

Implementing filtration structures can increase device fluidic resistance and can limit the device's ability to operate with low pneumatic pressures. The overall fluidic resistance of a filtration module can be reduced by a factor of n by maximizing the number of parallel orifices/filter channels (n), resulting in a local resistance of R_i/n , where R_i is the resistance of a single filter channel. The filter module in this work uses 100 parallel $15 \times 15 \mu\text{m}^2$ channels. This produces an equivalent effective resistance of 5.05×10^{12}

$\text{Pa}\cdot\text{s}/\text{m}^3$, while the fluidic resistance of a $200\times 40\ \mu\text{m}^2$ channel of equivalent length is comparable at $1.61\times 10^{12}\ \text{Pa}\cdot\text{s}/\text{m}^3$. The use of an in-line filtration module can drastically reduce the occurrences of constriction channel clogging and extend experiment duration. The filter modules summarized in Fig. 3(B) possess similar working principles of forcing samples to flow through arrays of small orifices of comparable size to the downstream constriction channel⁴⁰⁻⁴². The offset filter configuration has module inlets and outlets positioned rotationally symmetric from each other. As more filter orifices are clogged, there is an undesirable increase in fluidic resistance which should be minimized.

We first simulated fluid flow behavior for all filter configurations and determined which filter channels experience the largest volumetric flow. Secondly, we preferentially occluded filter channels to determine filter behavior over each filter's lifetime. An advantage of the offset configuration compared to existing filter configurations is the uniform pressure distribution across the length of the array (i.e., pressure drop is equal for all filter channels). This results in less severe resistance changes as increasingly more filter orifices/channels are occluded. At a 50% clogging state, the resistance of the offset design increases by 26.8% in comparison to 35.2%, 68.7% and 166% for other filter configurations. This improvement allows for more accurate fluidic handling for longer durations and increases total sample throughput.

Plug-in Ag/AgCl electrodes were used for measurement through fluidic reservoirs [Fig. 1(D)]. The implementation of filtration modules negatively obscures electrical measurement in traditional in-line plug-in electrodes used elsewhere^{34,43-45}. We reconfigured the electrode placement to maintain the simplicity of plug-in electrodes but still achieved the integration of filtration structures and circumvention of cell settling in electrode regions which plagued previous designs [see ESI Fig. 3(A)]. With the electrode placed perpendicular to the fluid flow direction and with the channel acting as a salt bridge, it remains electrically connected to measurement regions but experiences zero fluid flow under normal device operation. This also conveniently provides a reservoir for removing foreign debris which may have bypassed the filtration module and obstructed the constriction channel. While reversible flow has been

used to unclog microchannels^{46,47}, debris is still present within the fluidic network. Instead, we adjust the applied pressure on inlets to various states (-p, 0 or dead ended) and subtly redirect fluid flow, to flush debris into the electrode reservoir through the off-set channel. This provides an unclogging mechanism to extend measurement channel life by clearing obstructions [see ESI Fig. 3(C)].

In summary, maximizing parallel filter channels and employing a new 'offset' configuration minimize both the initial fluidic resistance and its undesirable increase over time. Plug-in electrodes share many technical advantages of 'parallel' electrodes, such as more accurate volume characterization and mimic the measurement configuration of 'aligned' electrodes. In addition, plug-in electrodes significantly reduce fabrication complexity⁴⁸. [see ESI Fig. 3(B)]. Integration of these electrodes into conventional microfluidics can be achieved by reconfiguring the electrode placement which conveniently promotes additional techniques for mitigating clogging of constriction channels. The combination of integrated filtration structures as part of sample preparation and an unclogging mechanism can be broadly applicable and enables downstream constriction channel operation for extended durations (e.g., measurement of ~10,000 cells per experiment).

Materials and Methods

Blood sample and reagent preparation

Blood samples were obtained from healthy donors via venipuncture (Mount Sinai Hospital, Toronto, Canada). Hematological parameters of whole blood samples varied within healthy physiological ranges (Lymph %: 8-32, WBC concentration: 10-13 cells/nL, MCV: 83-96 fL, RBC concentration: 3-5 cells/pL). Blood samples were anticoagulated with EDTA anticoagulant (ethylenediaminetetraacetic acid 1.5 mg ml⁻¹) (Sigma-Aldrich, Oakville, ON, Canada) and stored at room temperature prior to use within 12 hours of withdrawal. For each patient sample, an aliquot of the sample was also measured by a standard hematology analyzer (Sysmex XN-9000, Sysmex America, Illinois) for reference.

PBS with 1% w/v BSA (New England Biolabs Inc., Herts, UK) was used for device incubation and as RBC diluent. Lysis and quench solutions were prepared based on previously established bulk lysis protocols^{19,31}. Briefly, ~10 μ L of whole blood is mixed on-chip in a 1:12 ratio with lysis solution (0.12% v/v formic acid and 0.05% saponin in DI) and subsequently neutralized by 1:5.3 with a quench solution (0.6% w/v sodium carbonate in 1X PBS).

Device fabrication and operation

The device is composed of three separate areas each with distinct cross sectional dimensions, including the sample preparation and reagent handling channels (200 μ m \times 40 μ m), intermediate channels between electrodes (1,000 μ m \times 40 μ m), and constriction region for single cell measurement (15 μ m \times 15 μ m). The device is composed of three separate areas, each of which has different cross sectional dimensions, including the sample preparation and reagent handling channels (200 μ m \times 40 μ m), intermediate channels between electrodes (1,000 μ m \times 40 μ m), and constriction region for single cell measurement (15 μ m \times 15 μ m). Using standard soft lithography, two SU-8 layers were constructed on the mold master to provide 15 μ m and 40 μ m channel heights. Device molding involved a single layer of polydimethylsiloxane (PDMS) to achieve channels of multiple heights. Although the basal impedance is dependent on the geometric dimensions of the constriction channel (>50%), the intermediary channels also contribute substantial basal impedance and cannot be ignored.

Prior to experiments, devices were incubated with PBS, all inlets and outlets were sealed, and the device was pressurized to remove trapped gas pockets via diffusion through the PDMS channel wall. Whole blood, lysis and quench solutions were pipetted into their respective inlet ports/reservoirs. Two sets of Ag/AgCl electrodes, one for each measurement module, were plugged in the device. Sample and dilution outlets were then connected externally to a custom pneumatic pressure source that drives fluidic flow.

Signal processing

Sinusoidal voltages at multiple frequencies (10, 100, 400 and 990 kHz at 500 mV_{pp}) were applied through the Ag/AgCl electrodes. Entire impedance data files would be windowed into shortened segments, 7.2 kSa in length and processed sequentially. During signal processing for RBC analysis, WBCs and platelets were excluded based on distinct impedance signatures.

The inherent nature of a pressure-driven device is that zero gauge pressure is applied to the fluidic reservoirs and is subject to fluid evaporation over extended periods. Along with variability in post-lysis release of cellular components and cell densities, basal impedance could shift over time. Typical methods of detecting basal impedance are not suitable to use because of baseline shifting. Accordingly, we developed basal-histogram algorithm to correct for baseline shifting. This consists of first, fitting a low ordered polynomial to the windowed segment and secondly, subtracting the fit from the raw data. Without any corrections, baselines are often incorrectly calculated which causes numerous peaks at lower electrical volumes to be mis-identified as cells. Size measurement accuracy improves with the baseline correction as evidenced by the characteristic RBC distribution [see ESI Fig. 4(A)]. Basal impedance is extracted by calculating the maximum frequency (count) in a histogram of all baseline corrected impedance values [see ESI Fig. 4(B)].

Results and Discussion

Characterization of mixing ratios

The device was operated at varying pressures to determine its performance variation and to validate correct mixing ratios based on the circuit model analogy. Negative pressures ranging from 1,200 Pa to 2,100 Pa were applied via both the dilution and outlet ports. Two junctions (one RBC dilution step and RBC lysis) were observed via microscopy imaging to confirm agreement between experimental and theoretical mixing ratios. The mixing ratio was calculated by measuring the width of the merging fluidic

streams immediately adjacent to junction W_1/W_T (Fig. 4 Inset). Relative ratios of the fluid widths were directly correlated to their relative volumetric flow rate⁴⁹. Observing a location adjacent and downstream from the junction ensures that there is insufficient time and channel length to allow diffusion, and volumetric flow is reflected entirely in the measured ratio of fluid widths. The theoretical mixing ratios for a single RBC dilution step and RBC lysis are 1:10 (0.1) and 1:12 (0.083), respectively. The apparent mixing ratio remains relatively constant for both blood-lysis and blood-buffer mixing. The measured mixing ratio for all applied pressures was 0.11 ± 0.03 and 0.089 ± 0.012 for RBC and WBC junctions, respectively (Fig. 4).

Inherently linked to the applied pressure is the total volumetric flow through the device which varies proportionally to the applied pressure by a ratio (V/i_b) that is set during device design (see ESI Fig. 2). V and i_b denote voltage and current variables used in equivalent circuit model and are analogous to applied pressure and overall sample flow, respectively. Consequently, overall sample flow can be varied by modulating applied pressure while maintaining downstream mixing ratios. While the presence of this ratio (V/i_b) ensures the relative volumetric flow of each solution to remain constant, device operational success and accuracy deviates only at non-optimal pressures. Fluidic mixing relies on diffusion in the process of flowing through a long serpentine channel. For RBC lysis operated at 1,500 Pa, the average residence time in the fluidic mixing after introducing lysis solution was 5.8 s, enabling the lysis of approximately 6,000 RBCs. The whole blood mixture ideally requires 6 seconds of incubation to ensure complete lysis of RBCs.²⁵ At applied pressures of 1,800 and 2,100 Pa, the average residence time was 4.65 s and 4.01 s, which resulted in many un-lysed RBCs observed in both the filter and measurement regions.

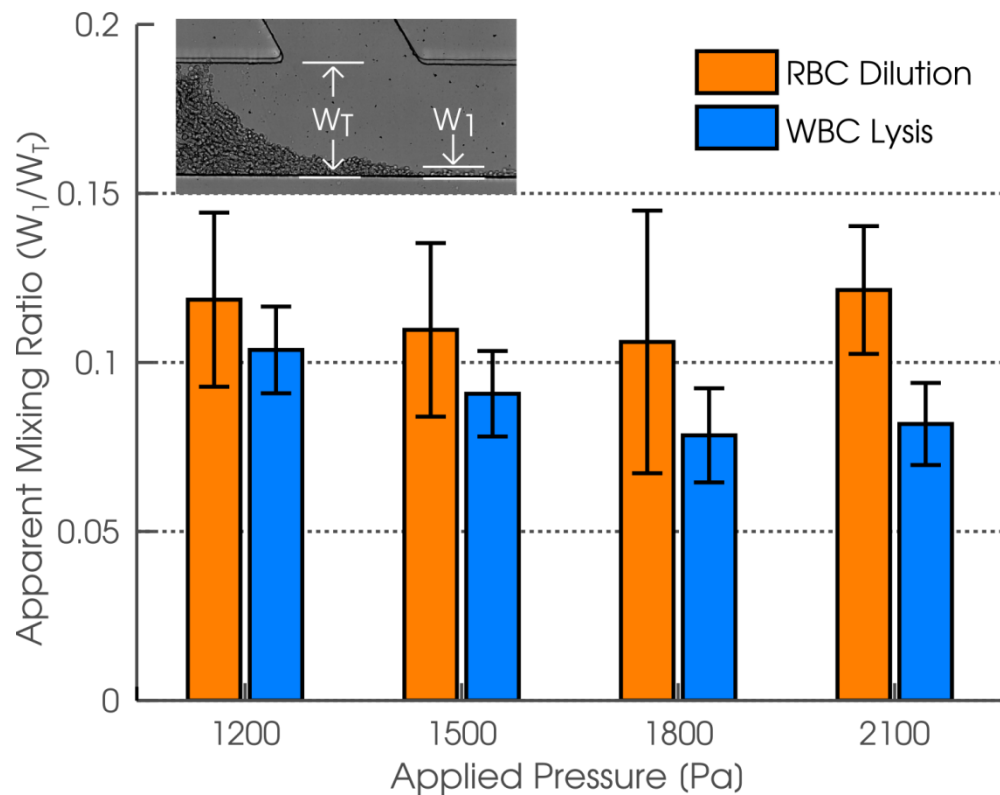


Fig. 4 Pressure variations do not significantly influence mixing ratios. The use of an inlet-outlet configuration for serial dilution is used to enable the device to behave consistently at different pressures. According to theoretical calculation, the expected mixing ratios are 0.1 and 0.083 for RBC dilution and RBC lysis, respectively. Experimentally measured mixing ratios for all applied pressures were 0.11 ± 0.03 and 0.089 ± 0.012 for RBC and WBC junctions ($n=3$) (Inset) Relative ratios of the fluidic widths (W_1/W_T) were correlated to their relative volumetric flow rate.

RBC enumeration and characterization

One critical component of complete blood counts is the enumeration and characterization of RBCs. In our work, RBC enumeration was conducted using various dilution ratios of 100 \times , 1,000 \times and 10,000 \times . Fig. 5(A) shows raw impedance data captured during one second of RBC measurement and the corresponding histogram from the cumulative measurement of $\sim 2,000$ cells. As expected, there were a high number of coincidence events at lower dilution ratios. Fig. 5(A) shows that size histograms for 100 \times

and 1,000× dilution ratios are right skewed and have a maximum frequency (%) at impedance values greater than the expected impedance change for RBCs. This combination confirms that multiple cells were incorrectly enumerated as a single large cell. For a dilution ratio of 10,000×, the system was able to reestablish an impedance baseline from which successive cells flowing through the measurement channel were detected. The absence of larger peaks >4 kΩ indicates minimal coincidence. The resultant size histogram concurs with reference hematology results in both distribution shape and mean.

The measured electrical volume is difficult to directly equate with its single cell volume when considering its resting biconcave shape and its deformed parachute shape in microfluidic channels³⁵. However, the electrical volume exhibited by a population of RBCs can be correlated to its mean cell volume, which is similar to the procedures performed in commercial hematology analyzers. Fig. 5(B) is an experimentally generated RBC size histogram showing various RBC indices that were measured. A high dilution ratio of 10,000× best mitigated the effect of RBC coincidence and produced results closest to reference RBC concentration benchmarked by the Sysmex commercial hematology analyzer. At 1,000× and 100× dilutions, the mistaken identification of multiple cells as a single cell resulted in much lower concentration measurement results. The stochastic nature of coincidence makes it difficult to adjust simply using a correction factor. The combined average standard deviation for dilution ratios of 1,000× and 100× was 1.076 cells/pL. A total of 104,735 RBCs from 10 samples were subsequently measured, and our devices produced concentration results with strong correlation with reference results ($R^2=0.83$) and an average difference of +0.1 cells/pL. Bias analysis also confirmed no skew or concentration dependent trend, highlighting the device's ability to conduct RBC dilution independent of native concentration and hematocrit.

Furthermore, mean corpuscular volume (MCV) was quantified by determining the mean value of the fitted Gaussian curve, while the distribution width (RDW-SD) was determined by the width of the fitting at 20% of the maximum height as per standardized hematology protocols for reading RBC volume histograms (Fig. 6(A)). As shown in Fig. 6(B), reference MCV measurements from Sysmex commercial

hematology analyzer and our device measured mean electrical volume for 10 patient samples were fitted, producing a correlation coefficient (R^2) of 0.97. The hematocrit of the tested blood samples encompassed a wide range varying from 32% to 46% , which highlights the device's ability to produce well correlated CV results independent of sample hematocrit..

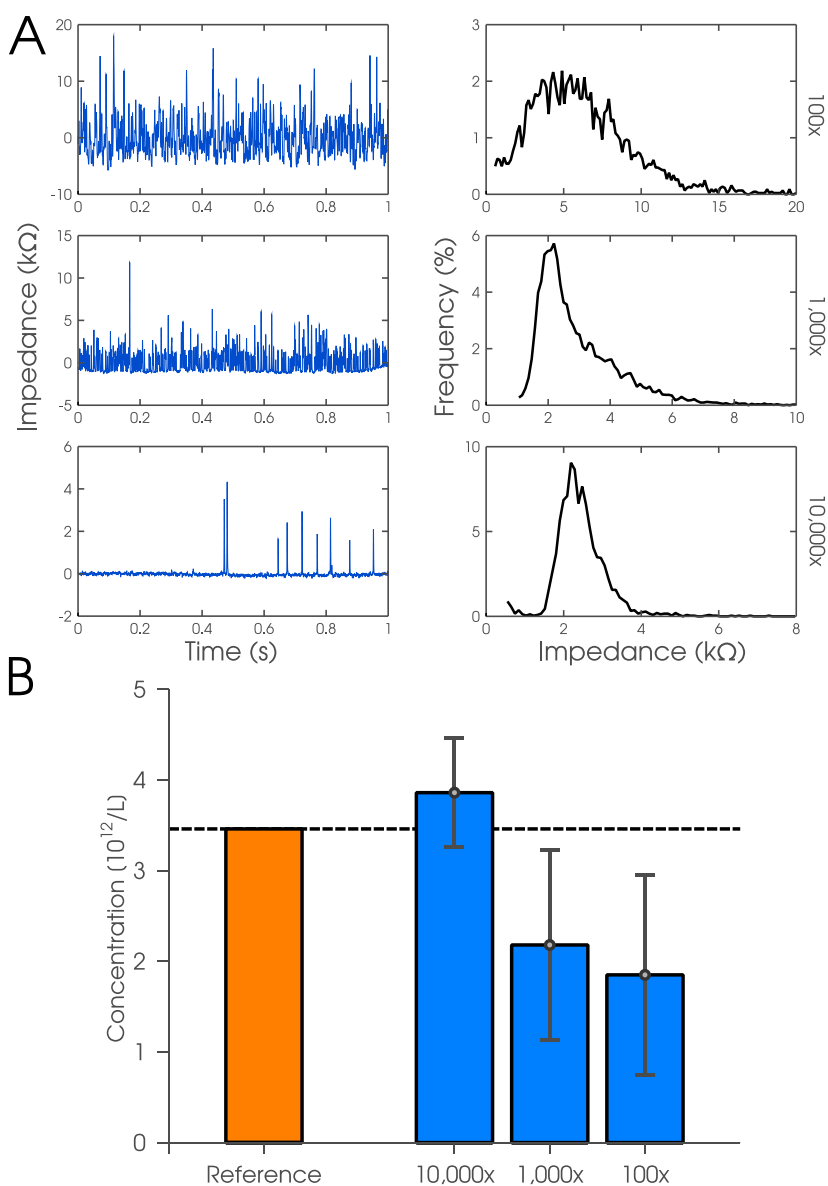


Fig. 5 Effect of dilution ratio on RBC enumeration. (A) 1 second window of raw data at varying dilution ratios (100×, 1,000×, and 10,000×) and corresponding accumulated impedance histograms for ~2,000 cells. 10,000× sample dilution allows for accurate detection of single RBCs. Both maximum values and

distribution shape of the size histogram indicate incorrect enumeration of clustered/coincident cells at lower dilution ratios. (B) Concentration measurement results at varying dilution ratios, compared with reference concentration measured by hematology analyzer.

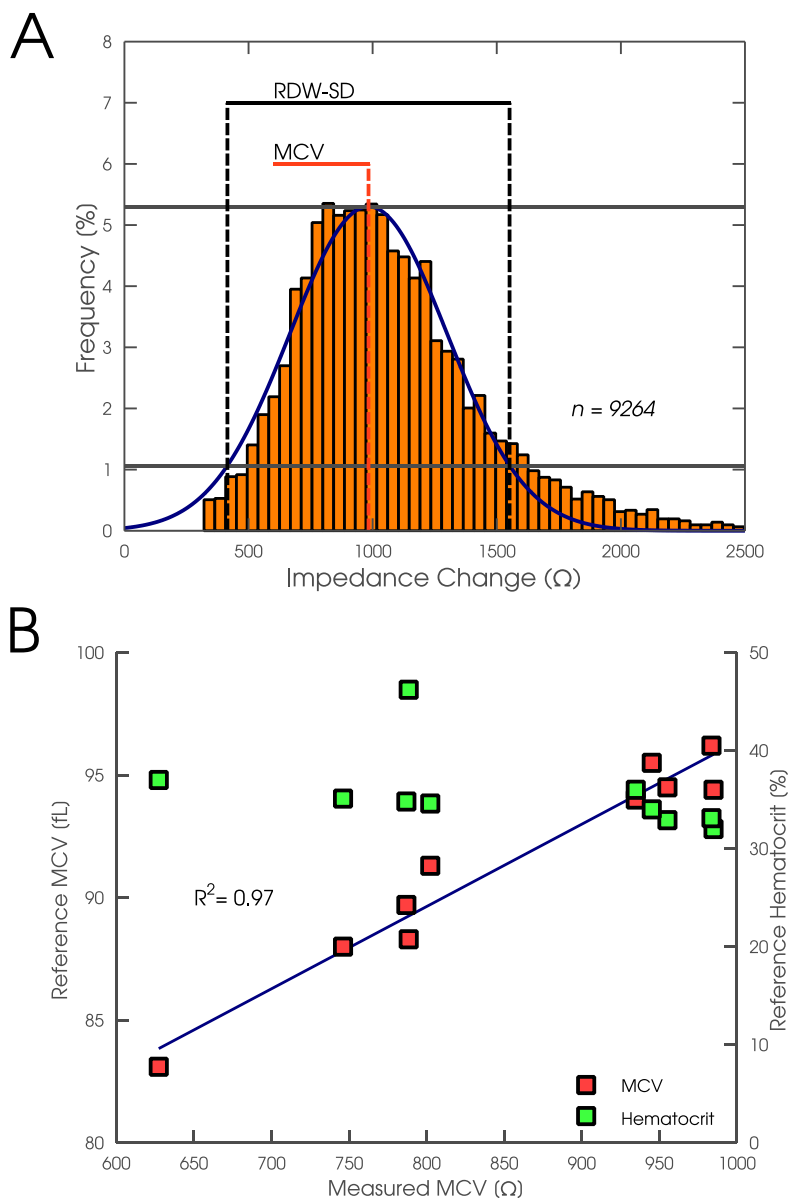


Fig. 6 RBC measurement results. (A) RBC size histogram highlighting measured RBC indices: distribution width (RDW-SD) and mean corpuscular volume (MCV). (B) Correlation plot for mean corpuscular volume (MCV): reference hematology analyzer (y) vs. microfluidically measured MCV (x). Line fitting generates a correlation coefficient of 0.97.

WBC enumeration and differential

There are two major WBC cell types, including lymphocytes and a grouped category of granulocytes and monocytes. We first confirmed the inherent cell diameter difference between lymphocytes and non-lymphocytes in a post-lysis sample using microscopy imaging [see ESI Fig. 5]. Measurement of cell diameter generated a bimodal distribution of WBCs, centered around 9 μm for lymphocytes and 14 μm for non-lymphocytes, which correlates well with volume differences of 70 fL and 210 fL respectively as determined by standard hematology analyzers⁵⁰.

Individually, RBC ghosts produce minimal electrical signals, but a relatively high concentration of RBC ghosts can collectively cause false identification with lymphocytes. Hence, our measurement used low and high frequency impedance data in tandem to selectively distinguish WBCs from RBC ghosts. Moderately high frequency impedance data (100-400 kHz) was used to identify WBC peaks and synchronized with both lower frequencies (10 kHz) and higher frequencies (990 kHz) to generate multi-frequency information. At lower measurement frequencies, impedance data most accurately reflects cell volume but is also most susceptible to false identification of RBC ghosts and debris. Higher frequencies provide impedance data that is dependent on both cell size and intracellular properties. At these frequencies RBC ghosts exhibit minimal electrical signatures and can easily be excluded from measurements. Opacity, which is the ratio of cell impedance at high frequency and low frequencies, is used to differentiate WBC subgroups.^{23,31,51}

Fig. 7(A) shows scatter graphs of low frequency (i.e., cell electrical volume) and opacity data for various lymphocyte ratios within and out of normal physiological ranges, measured on different samples. Opacity data here cannot conclusively differentiate between granulocytes and monocytes, but low frequency data in combination with high frequency data for cell identification from debris was sufficient to generate a predictable bimodal volume histogram and provided 2-WBC differentials. Minimal values in

the low frequency volume histograms shown in Fig. 7(A-Top) were identified as lymphocyte flags, and cells were categorized according to their relative position to these generated gating flags.

The microfluidic device performed on-chip raw blood processing and then conducted enumeration and size characterization of WBCs (97,305 total from 10 samples). Electrical measurements were compared to reference results from a standard hematology analyzer. Fig. 7(B)(C) show concordance (left) and Bland-Altman plots (right) for various blood cell parameters where the discrepancy between device and reference measurements is plotted against the average of the two ($n=10$). Bias and the 95% limits of agreement (LOA, $\text{bias} \pm 1.96\sigma$) are plotted in blue and red, respectively. WBC concentration measurements show a strong linear correlation ($R^2=0.94$) and has an average discrepancy that is close to zero (-0.5 cells/pL), as shown in Fig. 7(B). On average, there is a slight undercounting of WBCs by the microfluidic device relative to the reference hematology analyzer. The limits of agreement are relatively narrow [+0.0,-1.1] and is <16% of the healthy WBC concentration range³³. Device generated total WBC concentration and WBC differential bias values were within 4.5% and 6.8% of reference measurements. The device also shows the ability to accurately differentiate WBCs for lymphocyte ratios ranging from 8-32% with high correlation ($R^2=0.97$), as shown in Fig. 7(C).

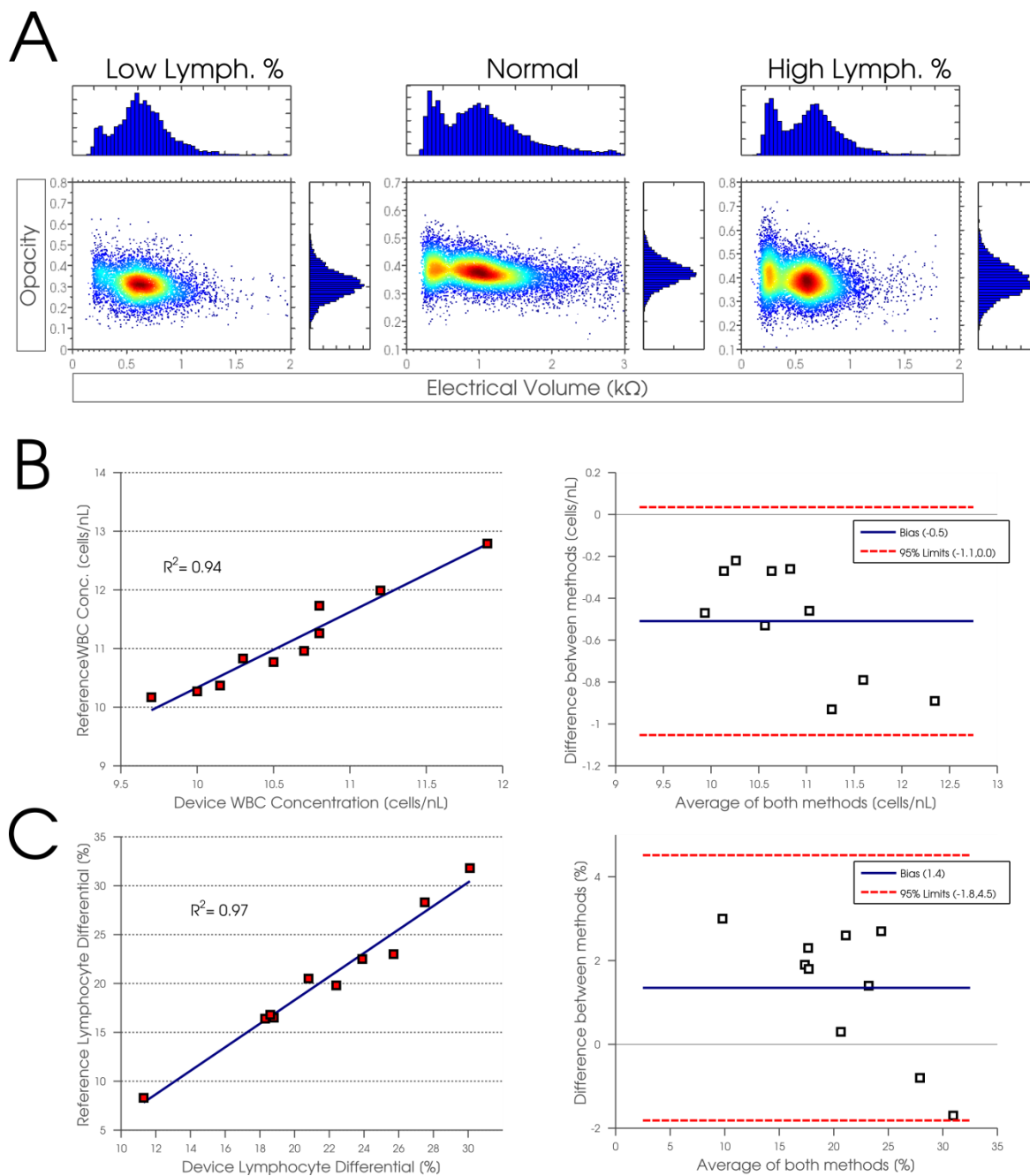


Fig. 7 WBC measurement results. (A) Scatter graphs showing opacity and electrical volume from patient samples of various lymphocyte populations. Abnormally low 8.3% (left), within healthy range 22.5% (center), and abnormally high 31.8% (right). (B) WBC concentration measurements. Correspondence (left) and Bland-Altman Plots (right). (C) WBC differential measurements for determining lymphocyte percent. Non-lymphocyte percent is (1-Lymph%).

Discussion

On-chip sample preparation on our device proved effective in both the dilution and lysis of RBCs to enable accurate enumeration of RBCs and WBCs. Final concentration results can be represented by $C = \frac{n}{f \cdot t} d_r$, where n is the number of detected cells, f is approximated flow rate, t is experiment duration, and d_r is the dilution ratio. Two major difficulties exist in predicting cell concentrations from electrical measurements. Firstly, it is important to accurately calculate the sample volume which can be estimated using the approximated flow rate and elapsed time. Both fluidic and electrical simulations rely on prior knowledge in fluid viscosities. Although blood viscosity is often approximated to be 5.3 Pa·s at room temperature (20°C), it is highly dependent on sample temperature²⁸ and can contribute to errors in flow approximation. While significant efforts were taken to ensure sample temperatures remained constant in our work, future work can include on-chip temperature control to mitigate this effect. Secondly, cell loss from sedimentation and unwanted chemical lysis can contribute to undercounting. Particularly in the analysis of WBC concentrations, the negative bias is indicative of a systematic trend. The relatively short constriction channel limits the maximum device flow rate which can promote cell sedimentation if cell velocities are too low^{52,53}. Strong linear correlations between device and reference results indicate the use of a correction factor or internal calibration can be used to account for cell loss from both sedimentation and chemical procedures. This is particularly applicable in a microfluidic environment due to its repeatable, uniform lysis and dilution conditions.

According to the Bland Altman plot in Fig. 7(C), there appears to be a negative sloped skew for WBC differential measurements. This deviation becomes more apparent in abnormally low or high lymphocyte percentages. Higher than expected lymphocyte percentages could be the consequence of lysis resistant RBCs being mistakenly enumerated as a small WBC.⁵⁴ The discrepancy between measurement techniques was consistently positive for low-normal lymphocyte percentages. Lymphocytes have been shown to slightly increase in average diameter while certain non-lymphocytes (neutrophils) have

decreased in diameter following treatment with saponin.³¹ The inherent overlap in diameters of non-lymphocytes and lymphocytes could be problematic in size differentiation. The systematic errors incurred are most likely inherent to the measurement mechanism and relying on size-only characteristics rather than the device's ability to perform controlled sample preparation.

Our difficulty in applying higher frequencies restricts the differential ability to perform 3-WBC categorization. As the device construction material, PDMS immediately adjacent to the constriction channel contributes a small parallel capacitance to the measurement circuit and limits our usable frequencies to the sub-MHz range. For frequencies in the MHz range, the generated size histogram from WBC analysis converges towards a single peak distribution. Opacity here cannot conclusively differentiate between granulocytes and monocytes, but low frequency data in combination with high frequency data for cell identification is sufficient to generate a predictable bimodal size histogram and provide 2-WBC differentials. Irrespective of these difficulties, the results from our microfluidic device measurement demonstrated strong linear correlation for WBC differential independent of initial lymphocyte or total WBC concentrations. The device design also proves the feasibility of performing whole blood pre-processing on chip to enable downstream measurements.

Conclusion

This paper reported a fully monolithic microfluidic system for simultaneously performing dilution and lysis of whole blood before conducting on-chip electrical enumeration and white blood cell differential. The filter and channel designs can be broadly applicable and can extend constriction channel lifetimes to enable the measurement of a high number of cells (e.g., over 10,000 cells). Raw blood samples from 10 patients were processed on chip and electrically analyzed on the device to measure several blood cell concentrations and parameters. Comparative results between reference hematology analyzers and the microfluidic device for specific RBC indices, RBC and WBC concentrations, and WBC differentials show strong correlations, proving the microfluidic device's capability to perform whole blood pre-

processing and measurement. More generally, the work demonstrates that this platform can be used to handle solutions of varied viscosities and mixing ratios and can provide sample preparation for single blood cell analysis as a monolithic device.

Acknowledgements

Financial support from the Government of Canada through Grand Challenges Canada is acknowledged. Authors also acknowledge financial support from Natural Sciences and Engineering Research Council of Canada (NSERC) via an NSERC E.W.R. Steacie Fellowship.

References

1. M. Shapiro and S. Greenfield, *Ann. Intern. Med.*, 1987, **106**, 65–74.
2. S. M. Lewis, B. Bain, and I. Bates, *Dacie and Lewis Practical Haematology*, Elsevier Ltd, Philadelphia, Tenth., 2006.
3. G. Dhaliwal, P. Cornett, and L. Tierney, *Am. Fam. Physician*, 2004, **69**, 2599–2606.
4. B. George-Gay and K. Parker, *J. Perianesthesia Nurs.*, 2003, **18**, 96–117.
5. T. D. Shanafelt and T. G. Call, *Mayo Clin. Proc.*, 2004, **79**, 388–98.
6. H. Lodish, A. Berk, L. Zipursky, P. Matsudaira, D. Baltimore, and J. Darnell, *Molecular Cell Biology*, W.H. Freeman, New York, 4th edn., 2000.
7. H. M. Ji, V. Samper, Y. Chen, C. K. Heng, T. M. Lim, and L. Yobas, *Biomed. Microdevices*, 2008, **10**, 251–7.
8. X. Chen, D. Cui, and J. Chen, *Electrophoresis*, 2009, **30**, 3168–73.
9. H. Wei, B. Chueh, H. Wu, E. W. Hall, C. Li, R. Schirhagl, J.-M. Lin, and R. N. Zare, *Lab Chip*, 2011, **11**, 238–45.
10. J. Alvankarian, A. Bahadorimehr, and B. Yeop Majlis, *Biomicrofluidics*, 2013, **7**, 014102.
11. A. J. Mach and D. Di Carlo, *Biotechnol. Bioeng.*, 2010, **107**, 302–11.
12. D. Di Carlo, D. Irimia, R. G. Tompkins, and M. Toner, *Proc. Natl. Acad. Sci. U. S. A.*, 2007, **104**, 18892–7.
13. L. Wu, G. Guan, H. W. Hou, A. A. S. Bhagat, and J. Han, *Anal. Chem.*, 2012, **84**, 9324–31.
14. S. Zheng, J. Liu, and Y. Tai, *J. Microelectromechanical Syst.*, 2008, **17**, 1029–1038.
15. M. Yamada and M. Seki, *Lab Chip*, 2005, **5**, 1233–9.
16. S. Shevkoplyas, T. Yoshida, L. Munn, and M. Bitensky, *Anal. Chem.*, 2005, **77**, 933–937.
17. Z. T. F. Yu, K. M. Aw Yong, and J. Fu, *Small*, 2014, **10**, 1687–703.
18. S. Yang, A. Undar, and J. D. Zahn, *Lab Chip*, 2006, **6**, 871–80.
19. Y. Li, C. Young, T. J. Fischer, J. H. Carter, and S. C. Veulens, 1998.
20. P. Sethu, L. L. Moldawer, M. N. Mindrinos, P. O. Scumpia, C. L. Tannahill, J. Wilhelmy, P. a Efron, B. H. Brownstein, R. G. Tompkins, and M. Toner, *Anal. Chem.*, 2006, **78**, 5453–61.
21. P. Sethu, M. Anahtar, L. L. Moldawer, R. G. Tompkins, and M. Toner, *Anal. Chem.*, 2004, **76**, 6247–53.
22. B. Ekberg, U. Larsen, and N. Fogh-Andersen, *Point Care*, 2005, **4**, 64–65.

23. X. Han, C. van Berkel, J. Gwyer, L. Capretto, and H. Morgan, *Anal. Chem.*, 2012, **84**, 1070–5.
24. N. N. Watkins, U. Hassan, G. Damhorst, H. Ni, A. Vaid, W. Rodriguez, and R. Bashir, *Sci. Transl. Med.*, 2013, **5**, 214ra170–214ra170.
25. U. Hassan, N. N. Watkins, C. Edwards, and R. Bashir, *Lab Chip*, 2014, **14**, 1469.
26. C. van Berkel, J. D. Gwyer, S. Deane, N. G. Green, N. Green, J. Holloway, V. Hollis, and H. Morgan, *Lab Chip*, 2011, **11**, 1249–55.
27. C. Kim, K. Lee, J. H. Kim, K. S. Shin, K.-J. Lee, T. S. Kim, and J. Y. Kang, *Lab Chip*, 2008, **8**, 473–9.
28. K. Hattori, S. Sugiura, and T. Kanamori, *Lab Chip*, 2009, **9**, 1763–72.
29. D. Irimia, D. a Geba, and M. Toner, *Anal. Chem.*, 2006, **78**, 3472–7.
30. G. M. Walker, J. Sai, A. Richmond, M. Stremmer, C. Y. Chung, and J. P. Wikswo, *Lab Chip*, 2005, **5**, 611–8.
31. D. Holmes, D. Pettigrew, C. H. Reccius, J. D. Gwyer, C. van Berkel, J. Holloway, D. E. Davies, and H. Morgan, *Lab Chip*, 2009, **9**, 2881–9.
32. B. Young, J. Lowe, A. Stevens, and J. Heath, *Wheater's Functional Histology: A Text and Colour Atlas*, Elsevier Health Sciences, 5th edn., 2006, vol. 14.
33. M. L. Turgeon, *Clinical Hematology Theory and Procedures*, Lippincott Williams & Wilkins, 5th edn., 2011.
34. Y. Zheng, J. Nguyen, C. Wang, and Y. Sun, *Lab Chip*, 2013, **13**, 3275–83.
35. Y. Zheng, J. Chen, T. Cui, N. Shehata, C. Wang, and Y. Sun, *Lab Chip*, 2014, **14**, 577–83.
36. K. W. Oh, K. Lee, B. Ahn, and E. P. Furlani, *Lab Chip*, 2012, **12**, 515–45.
37. C. J. Morris and F. K. Forster, *Exp. Fluids*, 2004, **36**, 928–937.
38. M. V Kameneva, M. J. Watach, and H. S. Borovetz, *Clin. Hemorheol. Microcirc.*, 1999, **21**, 357–63.
39. T. Tsuji, T. Sakata, Y. Hamaguchi, F. Wang, and B. Houwen, *Cytometry*, 1999, **37**, 291–301.
40. J. Chen, D. Chen, T. Yuan, X. Chen, Y. Xie, H. Fu, D. Cui, X. Fan, and M. K. Khaing Oo, *Microelectron. Eng.*, 2014, **128**, 36–41.
41. A. Carbonaro, S. K. Mohanty, H. Huang, L. a Godley, and L. L. Sohn, *Lab Chip*, 2008, **8**, 1478–85.
42. A. T. O'Neill, N. a Monteiro-Riviere, and G. M. Walker, *Lab Chip*, 2009, **9**, 1756–62.
43. Y. Zheng, E. Shojaei-Baghini, C. Wang, and Y. Sun, *Biosens. Bioelectron.*, 2013, **42**, 496–502.
44. J. Chen, Y. Zheng, Q. Tan, Y. L. Zhang, J. Li, W. R. Geddie, M. a S. Jewett, and Y. Sun, *Biomicrofluidics*, 2011, **5**, 14113.

45. Y. Zheng, E. Shojaei-Baghini, A. Azad, C. Wang, and Y. Sun, *Lab Chip*, 2012, **12**, 2560–7.
46. Y.-H. Chang, C.-J. Huang, and G.-B. Lee, *Microfluid. Nanofluidics*, 2011, **12**, 85–94.
47. S.-B. Huang, M.-H. Wu, and G.-B. Lee, *Sensors Actuators B Chem.*, 2009, **142**, 389–399.
48. S. Gawad, L. Schild, and P. H. Renaud, *Lab Chip*, 2001, **1**, 76–82.
49. S. Choi, M. G. Lee, and J.-K. Park, *Biomicrofluidics*, 2010, **4**.
50. Sysmex Xtra, *WBC Histogram Interpretations of 3-Part Differentiation*, 2011.
51. V. S. Hollis, J. a Holloway, S. Harris, D. Spencer, C. van Berkel, and H. Morgan, *PLoS One*, 2012, **7**, e43702.
52. J. Warrick, B. Casavant, M. Frisk, and D. Beebe, *Anal. Chem.*, 2011, **82**, 8320–8326.
53. Y. Zhang and S. Neelamegham, *Biophys. J.*, 2002, **83**, 1934–52.
54. M. Zandecki, F. Genevieve, J. Gerard, and a Godon, *Int. J. Lab. Hematol.*, 2007, **29**, 21–41.